Drivers of Ecosystem Stability Differ with the Intensity of Extreme Climatic Events

Aki Yanagawa[1], Rina Ueda[2], Sayaka Yoshikawa[3], Yoshihiko Iseri[4], and Sinjiro Kanae[5]

[1]School of Science and Engineering, Meisei University, 2-1-1 Hodokubo, Hino, Tokyo, 191-8506, Japan
5 [2]Nippon Koei Co., Ltd., 5-4 Kojimachi, Chiyoda-ku, Tokyo, 102-8539, Japan
[3]Institute of Integrated Science and Technology, Nagasaki University, 1-14 Bunkyo-cho, Nagasaki, 852-8131, Japan
[4]International Platform for Dryland Research and Education, Tottori University, 1390 Hamasaka, Tottori, 680-0001, Japan
[5]School of Environment and Society, Institute of Science Tokyo, 2-12-1 O-okayama, Meguro-ku, Tokyo, 152-8550, Japan

10 *Correspondence to*: Yanagawa A. (aki.yanagawa@meisei-u.ac.jp)

Abstract. This study investigates how the dominant drivers of ecosystem stability metrics vary across gradients of hydroclimatic extremity. While previous studies have documented the impacts of droughts and heavy rainfall on ecosystem functioning and resilience inferred from stochastic fluctuations, less attention has been given to whether the relative importance of climatic, biotic, and landscape controls changes systematically under different levels of climatic stress. To address this question, we quantified vegetation resistance and event-scale recovery responses and compared the contributions of meteorological, biodiversity, and topographic factors across a global range of hydroclimatic conditions. We find that under normal to moderately dry conditions, vegetation stability metrics are primarily associated with meteorological variables, particularly temperature and precipitation, consistent with earlier global assessments. Under severe and extreme drought conditions, resistance decreases markedly across most regions, whereas recovery responses exhibit weaker and more spatially heterogeneous changes. Importantly, in sparsely vegetated ecosystems such as grasslands and open shrublands, the relative dominance of drivers shifts from climatic to biodiversity and topographic factors under intensified drought stress, indicating context-dependent regulation of ecosystem stability. Deciduous needle-leaf forests show consistently low resistance and recovery capacity across climatic regimes, suggesting elevated sensitivity to hydroclimatic variability. Overall, our findings demonstrate that ecosystem stability under climatic extremes cannot be explained solely by meteorological forcing and highlight the increasing importance of biodiversity and landscape heterogeneity in shaping stability responses under intensifying climate variability.

1 Introduction

Ecosystem stability refers to the capacity of ecological systems to maintain and recover their functional integrity when exposed to environmental disturbances (Holling, 1973). Resistance and resilience, representing the degree to which ecosystems withstand perturbations and the extent of recovery following disturbance, respectively, remain foundational metrics for understanding ecological responses to ongoing global environmental change (Van Meerbeek et al., 2021). These concepts

provide a common framework for quantifying how ecosystems respond to and recover from external shocks. As climate change intensifies, extreme events such as severe droughts and heavy rainfall are becoming more frequent and severe (Ripple et al., 2024), increasing the need to assess resistance and resilience as key indicators of ecological vulnerability (Sun et al., 2022).

35   Recent advances in satellite remote sensing have enabled global assessments of vegetation stability across diverse ecosystems. Global-scale analyses using the Normalized Difference Vegetation Index (NDVI) time series have shown that vegetation sensitivity to climatic variability is widespread, with many ecosystems responding strongly to changes in water availability and temperature (Seddon et al., 2016). Additional work has demonstrated that resistance and resilience tend to be lower in regions experiencing substantial anthropogenic disturbance (Li et al., 2018). Other global studies have reported that evergreen

40   broadleaf forests maintain particularly high ecosystem stability, with species diversity contributing significantly to ecosystem stability in combination with radiation and temperature (Huang and Xia, 2019). More integrative modeling indicates that ecosystem stability emerges through interactions among climatic conditions, biodiversity, soil properties, and vegetation structural attributes, rather than through any single driver (Chen et al., 2021).

    In parallel, recent global assessments of vegetation resilience have increasingly focused on intrinsic system stability inferred

45   from stochastic fluctuations and autoregressive memory structures (Forzieri et al., 2022; Smith et al., 2022; Smith and Boers, 2023). While these approaches provide valuable insights into long-term stability dynamics, they primarily quantify system-level memory effects rather than recovery responses to discrete hydroclimatic events. In contrast, the present study quantifies event-scale resistance and recovery dynamics associated with explicitly defined climatic extremes. Because our primary focus is on nonlinear ecosystem responses to discrete hydroclimatic perturbations—such as droughts and excessive rainfall—we

50   adopt an event-conditioned evaluation framework that does not explicitly parameterize autoregressive processes, while recognizing that legacy and memory effects remain embedded in ecosystem states and may implicitly shape observe responses. Collectively, these studies highlight the multifactorial nature of ecosystem stability, but they share several important limitations. First, most previous global assessments have not evaluated how the dominant drivers of stability change across different intensities of climatic extremes. Analyses typically evaluate stability under average or static climatic contexts, without

55   distinguishing between normal, moderate, and severe-to-extreme drought and wet conditions. This represents a critical gap, because ecosystems often exhibit nonlinear or threshold-type responses under extreme climatic stresses that differ fundamentally from responses observed under normal climatic conditions. Such nonlinear responses have been hypothesized in ecological theory, where ecosystems may remain relatively stable up to a critical stress level and then shift rapidly once that threshold is exceeded (e.g., alternative stable states and ecological thresholds frameworks). In addition, empirical and

60   conceptual research suggests that variation in species-level responses to environmental change—so-called response diversity—is a key determinant of how ecological communities respond to increasing stress, and the loss of such response diversity can lead to abrupt declines in ecosystem resilience rather than gradual changes (Mori et al., 2013). For example, this previous research provides a conceptual model showing that when species vary in their sensitivity to stressors, community-level functions can be maintained until compensatory dynamics break down, potentially resulting in threshold-like system

65   responses. These findings highlight the importance of considering nonlinear and threshold dynamics when evaluating ecosystem stability across climatic extremes.

Second, key non-climatic controls, such as biodiversity, soil properties, and land-use history, have rarely been integrated comprehensively. Land management intensity has been shown to modify biodiversity–resilience relationships, with positive effects emerging only under the strongest management regimes, whereas drought resistance has been associated more strongly

70   with mowing frequency than with species richness (Vogel et al., 2012). Long-term land-use history has been linked to variation in resistance through its influence on plant functional traits (Adler et al., 2004). Soil conditions, including moisture, carbon content, and bulk density, have also been identified as important but underexplored determinants of stability (Berdugo et al., 2022; Wei et al., 2025). In addition, topographic factors such as elevation, slope, and aspect regulate microclimatic conditions, soil water redistribution, and solar radiation, thereby modulating vegetation exposure and sensitivity to climatic extremes.

75   These terrain-driven controls can amplify or buffer drought and heat stress at local scales, yet they are often overlooked in large-scale assessments of ecosystem resistance and resilience.

Despite these findings, no previous global analysis has simultaneously incorporated climatic variables, biodiversity metrics, anthropogenic species gains and losses, soil properties, topographic factors, and land-use histories within a unified framework. Equally important, no prior study has examined whether—and how—the relative importance of these drivers changes

80   systematically with the severity of climatic extremes, such as those defined by the Standardized Precipitation–Evapotranspiration Index (SPEI). Consequently, predictions of ecological vulnerability under future climate scenarios remain limited.

To address these gaps, the present study investigates how the dominant drivers of vegetation resistance and resilience vary across a full gradient of drought and wetness severity categories. Using satellite-derived NDVI data, hydroclimatic

85   characterization based on SPEI, and a machine-learning approach (LightGBM), the present study evaluates the relative contributions of climatic variables, biodiversity metrics (including anthropogenic species increases and losses), soil properties, elevation, irrigation intensity, and long-term land-use histories across diverse land-cover types and hydroclimatic regimes.

This integrated approach allows us to determine whether ecosystem stability is governed primarily by climatic drivers under moderate conditions, but shifts toward biotic and structural controls under extreme conditions. By explicitly stratifying

90   analyses across multiple climate-extreme categories and incorporating a uniquely comprehensive set of explanatory factors, this study provides a new multidimensional perspective on how ecosystems respond to increasingly frequent and intense climatic extremes.

Our findings offer an improved and more comprehensive predictive understanding of global patterns of ecological vulnerability and have important implications for designing climate-specific and ecosystem-specific management and conservation

95   strategies aimed at sustaining ecosystem functioning in an era of accelerating climate change.

2 Materials and Methods

2.1 Overview of the Analytical Workflow and Spatiotemporal Scales

Global datasets harmonized to a 5° × 5° spatial grid were first divided by land-cover type and then assigned to climate-event classes. Fig. 1 (left) outlines the workflow for land-cover classification, and Fig. 1 (right) summarizes the datasets and their functions. The datasets used in the analysis were divided into three groups: (1) those used to derive the response variables (resistance and resilience), (2) those used to compute explanatory variables, and (3) those used for classification (land cover and SPEI).

All datasets were harmonized to a 5-min spatial resolution. Time-series analyses were conducted over the period 1982–2015, excluding 1990–1994. NDVI during this interval was influenced by NOAA-11 orbital drift, which shifted the satellite's equatorial crossing time by ~3.7 hours (Li and Brown, 2017) and altered the solar geometry during acquisition. This period also included the Pinatubo eruption, thereby introducing additional radiative anomalies. To avoid these confounding effects, NDVI data for 1990–1994 were removed, and all analyses were conducted for 1982–1989 and 1995–2015. As NDVI quality declines at high latitudes, the analysis domain was restricted to 60° N–60° S (Beck et al., 2006; Justice et al., 1985).
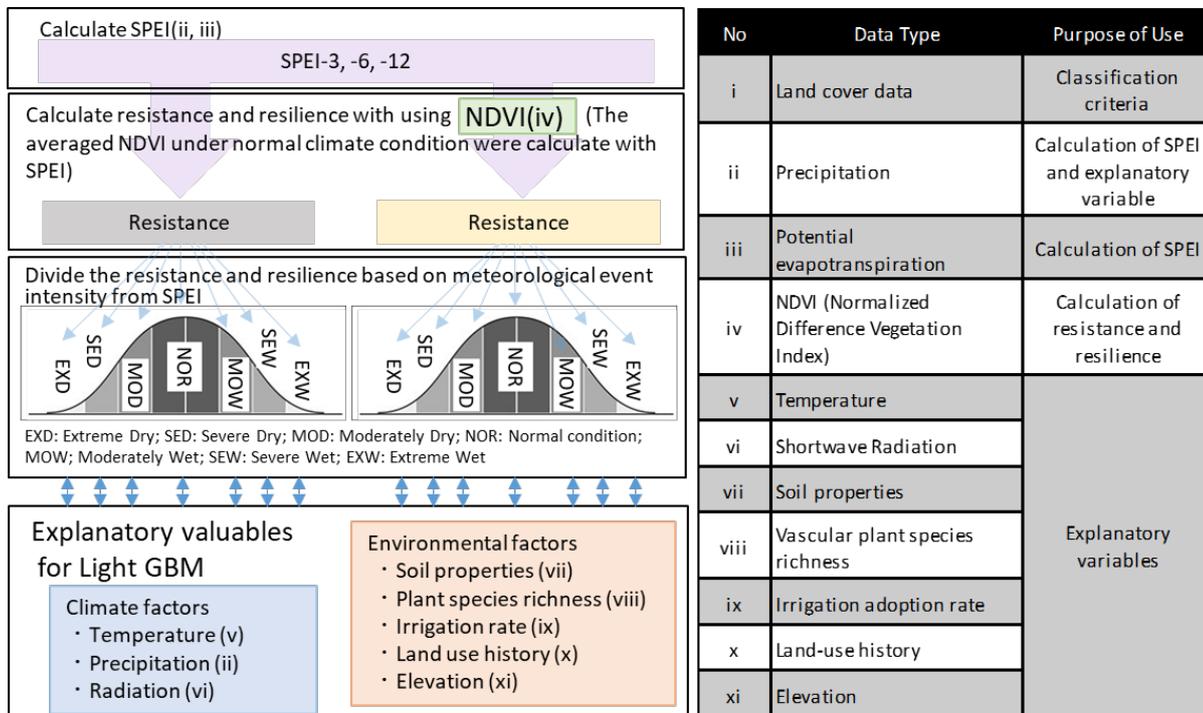

Figure 1. Left: Analytical workflow illustrating the processing steps applied after all grid cells were first classified by land-cover type, with subsequent analyses conducted separately for each land-cover class. The left panel also shows the use of SPEI at 3-, 6-, and 12-month accumulation time scales (SPEI-3, SPEI-6, and SPEI-12), representing short-term, seasonal, and annual

water-balance conditions, respectively. Right: Datasets and their roles in the analysis. Greek numerals in the left panel correspond to the items listed on the right. Item i (land-cover data) is not shown in the left panel because land-cover classification was performed as a prerequisite step, and all subsequent analyses were conducted independently within each land-cover category. In total, the modeling framework encompassed multiple combinations of land-cover types, climatic time scales, climate-event classes, and response metrics. Specifically, resistance and resilience were calculated for 11 land-cover classes, three SPEI accumulation time scales (SPEI-3, SPEI-6, and SPEI-12), and seven climate-event categories defined separately for each SPEI time scale. As both resistance and resilience were evaluated for each combination, this design resulted in $11 \times 3 \times 7 \times 2 = 462$ individual models, all of which were analyzed to assess ecosystem responses to climatic extremes.

2.2 Site Selection

Terrestrial regions worldwide were included, except for land-cover types represented by very few grid cells (Channan et al., 2014). The excluded classes were Closed Shrublands (CS), Permanent Wetlands (PW), Urban and Built-up areas (U), Barren land (B), and Snow and Ice (SI). The retained land-cover classes included Evergreen Needleleaf Forest (ENF), Evergreen Broadleaf Forest (EBF), Deciduous Needleleaf Forest (DNF), Deciduous Broadleaf Forest (DBF), Mixed Forest (MF), Open Shrublands (OS), Woody Savannas (WS), Savannas (S), Grasslands (G), Croplands (C), and Cropland/Natural Vegetation Mosaic (C/N). Land-cover data were used at a 5-minute spatial resolution.
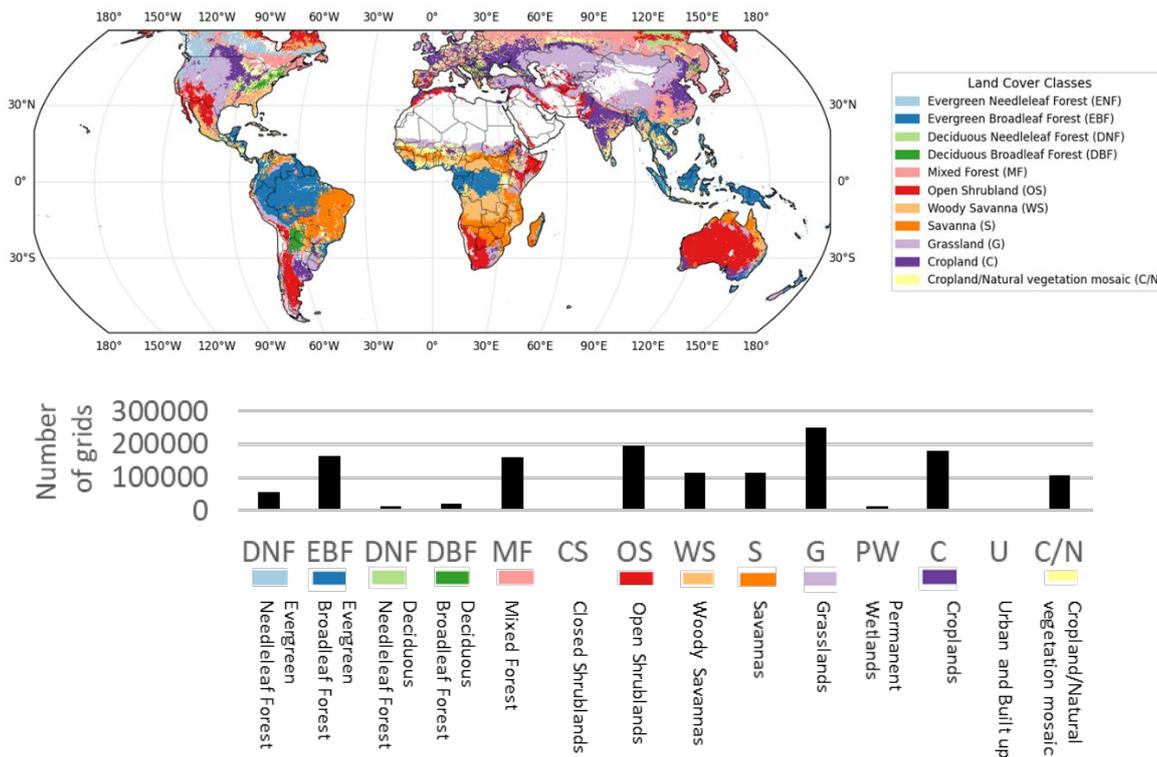
Figure 2. Spatial distribution of each land-cover type (upper figure) and the corresponding number of grid cells (lower graph). The lower bar chart represents the total number of grid cells for each land-cover type. Among them, CS, PW, and U were excluded from the analysis because the number of grids in these categories was extremely small. In addition, although not shown here, Barren areas—regions with almost no vegetation—were also excluded from the analysis. On the global map, only the land-cover types included in the analysis are color-coded.

2.3 Classification of Climate Conditions

The climate conditions for each grid cell were classified using the Standardized Precipitation–Evapotranspiration Index (SPEI, Vicente-Serrano et al., 2010) at 3-, 6-, and 12-month time scales for 1982–2015. Seven categories were defined (Fig. 3): extremely dry (SPEI < –1.645), severely dry (SPEI < –1.28), moderately dry (SPEI < –0.67), normal (–0.67 ≤ SPEI < 0.67), moderately wet (SPEI > 0.67), severely wet (SPEI > 1.28), and extremely wet (SPEI > 1.645). These thresholds correspond to the probabilities under a standard normal distribution.

SPEI was computed using the SPEI R package (Begueria and Vicente-Serrano, 2017) using precipitation from GPCC v7.0 (1° resolution; Schneider, 2015) and potential evapotranspiration from CRU-TS 4.01 (0.5° resolution; University of East Anglia Climatic Research Unit et al., 2017). To obtain complete time series across all SPEI scales, climate data from 1981 to 2015 were used. SPEI results were then aligned with the NDVI datasets after the removal of 1990–1994.
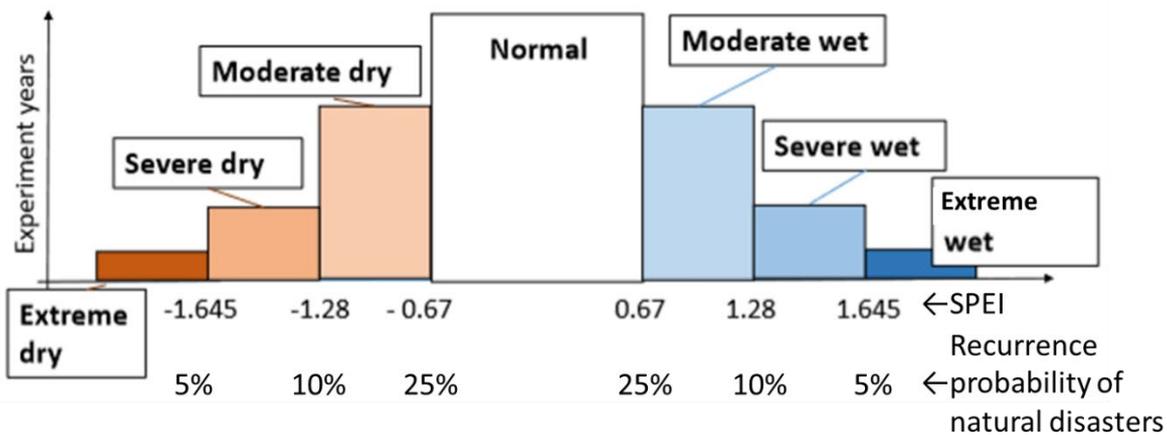
Figure 3. Classification of seven climate conditions based on SPEI. SPEI is an index derived from a probability distribution, meaning that its values correspond directly to probabilities under a standard normal distribution. An absolute value of 1.645 represents a 5% probability level. In this study, we classified climatic conditions with absolute SPEI values greater than 1.645 as extreme events, which occur with a probability of less than 5%, or roughly once every 20 years. Similarly, climatic conditions with absolute SPEI values between 1.28 and 1.645 correspond to a 5–10% probability range and were classified as severe events. Conditions with absolute values between 0.67 and 1.28 correspond to a 10–25% probability range and were

6

155   classified as Moderate events. All remaining values were categorized as Normal conditions, which occur with a probability of approximately 50%, representing climatic conditions that are expected to occur roughly once every two years.

2.4 Calculation of Resistance and Resilience

Resistance and resilience were derived from the NDVI3g dataset (GIMMS; Mao and Yan, 2019) at a 5-minute resolution. NDVI from 1990 to 1994 was excluded. The maximum biweekly NDVI value was retained for each month. For each grid cell,

160   the month that most frequently contained the annual NDVI maximum between 1982 and 1989and between 1995 and 2015 was identified (Fig. 4). This "peak month" was treated as a proxy for the annual vegetation productivity.

Resistance and resilience were defined as follows:

$$Resistance = \frac{1}{(NDVI_m - NDVI_e) + 1} \tag{1}$$

$$Resilience = \frac{1}{(NDVI_m - NDVI_{e+1}) + 1} \tag{2}$$

165   where $NDVI_m$ is the mean NDVI in normal years ($-0.67 \leq SPEI < 0.67$), $NDVI_e$ is the NDVI during the climate-event year, and $NDVI_{e+1}$ is the NDVI in the year after the event.

Autoregressive formulations were not used because the analysis incorporated categorical and non-time-series explanatory variables.
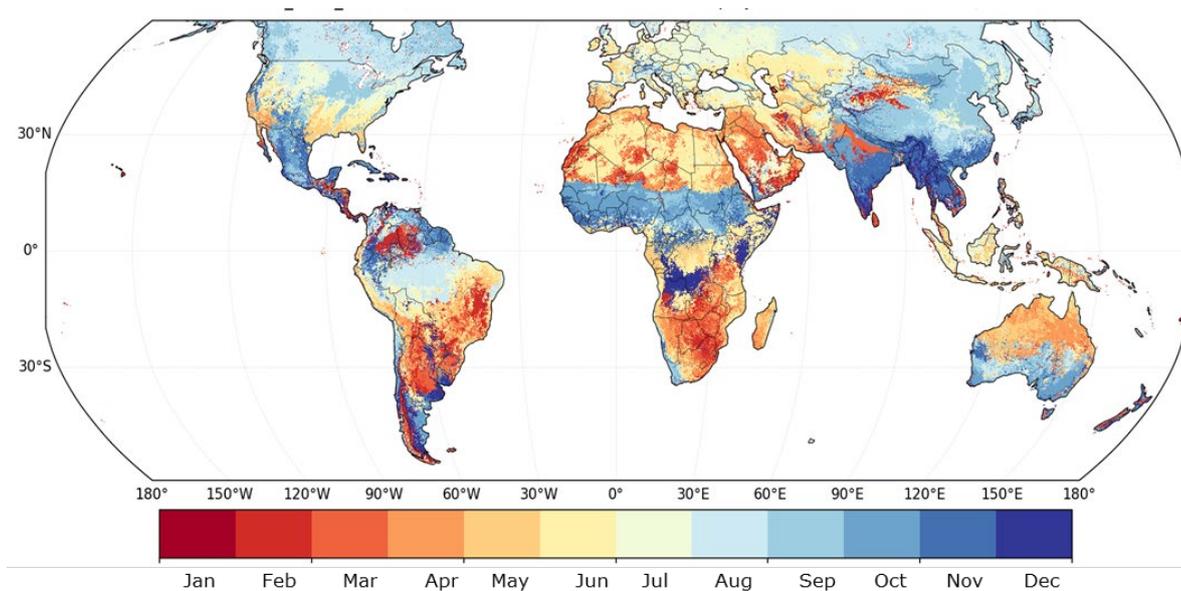
170

Figure 4. The month detected for each grid. The Detected Month represents the month in which the annual maximum NDVI most frequently occurred during the analysis period for each grid cell. Specifically, for each year, the month with the highest monthly NDVI was identified, and the frequency of these peak-NDVI months was counted across all years. The month with

175 the highest occurrence was then assigned to each grid cell. The figure shows these results using a color-coded scheme, where the numbers 1–12 correspond to the calendar months.

2.5 Explanatory Factors

Twenty-two explanatory variables were compiled and grouped into four categories: climatic, abiotic, biodiversity-related, and
180 land-use history/irrigation variables (Table 1 and Supplementary Information: Rationale for Selecting Explanatory Variables).
Climatic Factors: Annual precipitation (P: Schneider, 2015), temperature (T: University of East Anglia Climatic Research Unit et al., 2017), and shortwave radiation (R: European Centre for Medium-Range Weather Forecasts, 2012) were obtained for the event year, the preceding year (–1), and the following year (+1). The +1 variables were used only for resilience models, yielding 19 explanatory variables for resistance and 22 for resilience models.

185 Abiotic Factors: Elevation (Fischer et al., 2008) and six soil properties (Global Soil Data Task Group, 2000)—bulk density, wilting point, plant-available water capacity, thermal capacity, soil organic carbon, and soil nitrogen—were included because of their roles in water and nutrient regulation.

Biodiversity-Related Factors (Ellis et al., 2012): Anthropogenic species increase (ASI) was estimated using alien species distributions, crop species data, and urban area extent. Anthropogenic species loss (ASL) was derived from vegetation patterns
190 and habitat-based models. Anthropogenic species richness (ASR) was calculated as follows:

$$ASR = N\text{-}ASL + ASI \tag{3}$$

where N is the potential species richness, estimated using the global model by Kreft and Jetz (2007).

Land-Use History and Irrigation: HYDE 3.1 data (Klein Goldewijk et al., 2011) were used to estimate the duration (years) that each grid cell had been under cropland or pastureland for the past 8,000 years. The extent of irrigation was obtained from the
195 Global Map of Irrigation Areas (Siebert et al., 2013).

2.6 Normalization of Explanatory Variables

Non–time-series variables (soil, elevation, land-use history, ASR/ASI/ASL) were normalized to a 0–1 scale using the global minimum and maximum values:

200
$$Y = \frac{X - X_{mean}}{X_{Max} - X_{Min}} \tag{4}$$

X: Data for any given grid

Y: Normalized data (0–1 range) for the corresponding grid

X_{mean}: Mean value across all grids

X_{Max}: Maximum value across all grids

205 X_{Min}: Minimum value across all grids

Time-series climatic variables (T, P, R) were aggregated to annual values and normalized within each grid cell across 1982–1989 and 1995–2015 as follows:

$$Y_i = \frac{P_i - P_{mean}}{P_{Max} - P_{Min}} \tag{5}$$

P_i: Data for year **i**

Y_i: Normalized data (0–1 range) for year **i**

P_{mean}: Mean value across all years

P_{Max}: Maximum value across all years

P_{Min}: Minimum value across all years

Grids outside 60° N–60° S were excluded because of NDVI reliability limitations.

2.7 Modeling Approach

The relationship between the explanatory variables and vegetation resistance or resilience was assessed using a Light Gradient Boosting Machine (LightGBM) model (Shi et al., 2025). LightGBM was selected because it can efficiently capture nonlinear relationships and interaction effects among multiple climatic drivers without requiring a priori assumptions about functional forms, which is particularly important for ecosystem–climate analyses where threshold behavior and scale-dependent responses are common. In addition, its histogram-based learning algorithm and leaf-wise tree growth strategy enable high computational efficiency, making it well suited for large-scale, high-dimensional environmental datasets.

Another advantage of LightGBM is its robustness to multicollinearity among predictors, such as correlated climate variables or indices at different accumulation time scales, allowing all explanatory variables to be retained without prior dimensionality reduction. Furthermore, LightGBM can internally handle missing values by learning optimal split directions for missing observations, which reduces the need for explicit gap-filling procedures and improves robustness when working with long-term remote-sensing and climate datasets. The models were trained using a 70/30 split with up to 1000 iterations, with early stopping every 100 iterations when the prediction accuracy no longer improved. Model performance was evaluated using the root mean square error (RMSE) and coefficient of determination (R^2).

To quantify the relative contribution of individual explanatory variables, feature importance was evaluated using the gain metric:

$$Feature\ Importance\ (Gain)_j = \sum_{t \in T_j} \Delta Loss_t \tag{6}$$

where T_j denotes the set of decision tree splits that involve feature j, and $\Delta Loss_t$ represents the reduction in the loss function attributed to split t. Because this metric directly reflects the degree to which each variable contributes to reducing the model error, it is widely regarded as a highly practical and interpretable indicator of variable influence in gradient boosting models.

Table 1. Explanation of valuables in Light GBM

Explanately valuables	Abbrevi-ation	Explanation

Temperature[a] (℃)	T-1	The cumulative temperature of the year preceding the target climatic event
	T	The cumulative temperature in the year of the target climatic event
	T+1	The cumulative temperature in the year following the target climatic event
Precipitation[b] (mm/month)	P-1	The cumulative precipitation in the year preceding the target climatic event
	P	The cumulative precipitation in the year of the target climatic event
	P+1	The cumulative precipitation in the year following the target climatic event
Radiation[c] (W m^{-2})	R-1	The cumulative short radiation in the year preceding the target climatic event
	R	The cumulative short radiation in the year of the target climatic event
	R+1	The cumulative short radiation in the year following the target climatic event
Species richness[d] (number)	ASR	Anthropogenic Species Richness
	ASI	Anthropogenic Species Increase
	ASL	Anthropogenic Species Loss
Land use history[e] (Year)	Grass	Number of years each grid cell experienced grazing over 20 km² (6000 BCE–2000 CE)
	Crop	Number of years each grid cell experienced cropping over 20 km² (6000 BCE–2000 CE)
Irrigation[f](%)	Ir	The proportion of irrigated land area relative to the total area of the grid cell
Elevation[g](m)	El	Median elevation above sea level
Soil properties[h]	Ca	The total mass of organic carbon in a given soil-depth interval (g/m^{-2})
	N	The nitrogen content (% by weight) of a given soil-horizon (%)
	Bk	Bulk density at soil depths from 0 to 100 cm (g/cm³)
	Wp	Soil water content retained within the 0–100 cm soil profile at a pressure of –1500 kPa (m³ m^{-3})
	Thrcap	Soil thermal capacity at soil depths from 0 -100 cm (J m^{-2} K^{-1})
	Pawc	Soil water content retained within the 0–100 cm soil profile at a pressure of –10 kPa (m³ m^{-3})

Note. All time-series datasets were analyzed for the target periods of 1982–1989 and 1995–2015, and were resampled to a uniform spatial resolution of 5 min. Although the original datasets were provided in different physical units, all variables were normalized to a common 0–1 range prior to analysis to ensure comparability among predictors.

240   [a]University Of East Anglia Climatic Research et al. (2017). [b] Schneider et al. (2015). [c]European Centre for Medium-Range Weather Forecasts (2012). [d]Ellis et al. (2012). [e] Klein Goldewijk et al. (2011). [f]Siebert et al. (2013). [g]Fischer et al. (2008). [h]Global Soil Data Task Group (2000).

3 Results

3.1 Variation in Vegetation Resistance and Resilience with SPEI Severity of Extreme Events

Fig. 5 shows the resistance and resilience estimated from SPEI-3, separated by climatic conditions, with results for extreme drought and extreme wet conditions across all land cover types. Fig. 6 shows the spatial distribution of resistance and resilience based on SPEI-3 for all climate categories. The full set of results for all SPEI timescales and climatic conditions is presented in Fig. S2–S4.

In Fig. 5, the median values indicate that, under both drought and wet conditions, deciduous needle leaf forests (DNF) exhibit low resistance and low resilience under extreme drought conditions. Open shrublands (OS), grasslands (G), and croplands (C) also showed resistance and resilience values below 1 under extreme drought conditions, similar to DNF, but their resilience values were not as low as those of DNF.

Drought-related patterns in Fig. 6a and 6b show that resistance declines most strongly in dryland regions, especially in areas classified as grasslands (light purple) and savannas (orange) in Fig. 2. These regions include sub-Saharan Africa, the interior of the Eurasian continent, and the central Great Plains of North America, where resistance markedly decreases. Reductions in resilience were weaker and less spatially coherent than those in resistance. Under wet conditions, partial decreases in resistance appear in some high-latitude and temperate regions. By stratifying resistance and resilience according to the climate category, the maps revealed that ecosystem responses to extreme events vary strongly among regions (Fig. 6), underscoring the need to compare ecosystem stability under comparable climatic conditions rather than assuming spatially uniform responses.

3.2 Drivers of Resistance and Resilience Identified by LightGBM

For each of the 11 land cover types, the most important variables in the LightGBM models for resistance and resilience were identified across three reference periods (SPEI-3, -6, and -12 months) and seven water balance categories (Table 2). A total of 462 model results were obtained. In all cases, the root mean square error (RMSE) between the predicted and observed values was < 0.05, whereas the coefficient of determination (R^2) varied among the models (Fig. 7). In Table 2, the variables with the highest feature importance are highlighted in bold only when $R^2 > 0.5$ (e.g., Fig. 7a). The background pattern of each cell indicates the magnitude of resistance or resilience. Values between 0.99 and 1 (inclusive of 0.99 and exclusive of 1) are shown with light diagonal hatching slanting downward to the right. Values greater than 1 and up to 1.01 (inclusive of 1 and 1.01) are indicated with a gray background. Values below 0.99 are represented by dark diagonal hatching slanting downward to the right, whereas values above 1.01 are shown with dark diagonal hatching slanting upward to the right.

The analysis was stratified by SPEI calculated over 3-, 6-, and 12-month time scales, and the feature importance of each explanatory variable in the LightGBM models for resistance and resilience was summarized for each land cover type and climate category (Fig. S5–S6).

Fig. 7a and 7b show the minimum and maximum R^2 values, respectively, among all the resistance and resilience models. Panel (a) represents the resistance of DNF under Extreme drought conditions based on SPEI-3. Panel (b) shows the resilience of the

EBF under Normal conditions based on SPEI-6. The following subsections discuss (i) drivers under normal conditions, (ii) models that do not meet the criteria $R^2 > 0.5$ and variation in resistance or resilience > 0.01, and (iii) models in which $R^2 > 0.5$ and variation in resistance or resilience exceeds 0.01.

3.2.1 Drivers under Normal Climate Conditions

280 Under Normal climatic conditions, temperature-related variables were consistently identified as the dominant drivers of ecosystem stability, with the exception of resilience in DNF under SPEI-12, for which R+1 had the highest importance. For resistance, the temperature in the previous year (T−1) was the most frequently selected driver, appearing in 18 of the 33 combinations (≈54.5%). For resilience, the temperature in the recovery year (T+1) was selected in 16 combinations (≈48.4%). These patterns indicate the predominant role of temperature in regulating ecosystem stability under normal conditions. The

285 temporal shift in the temperature effects aligns with the functional difference between the two stability components: resistance, which reflects susceptibility to impact, is more strongly influenced by pre-event temperature, whereas resilience, which reflects recovery capacity, is more strongly associated with temperature in the year following the event.

3.2.2 Models Not Meeting the Criteria $R^2 > 0.5$ and Variation > 0.01

For ENF, EBF, and WS, no cases met the thresholds of $R^2 > 0.5$ and variation in resistance or resilience > 0.01 for any response

290 variable. This pattern suggests that these land cover types did not exhibit a clear, consistent response to climate extremes, such as severe droughts or heavy rainfall.

For EBF, all LightGBM models yielded $R^2 < 0.5$, which may reflect either the insufficient explanatory power of the environmental variables used in this study or the inherently small variation in resistance and resilience. In contrast, ENF and WS showed $R^2 > 0.5$ under some Extreme or Severe drought or wet conditions, and in most of these cases, temperature-related

295 variables had the highest feature importance.

### 3.2.3 Models with $R^2 > 0.5$ and Variation in Resistance or Resilience > 0.01

For DNF, DBF, and MF, several cases under severe drought or wet conditions exhibited $R^2 > 0.5$. Across these forest-dominated land cover types, climate variables were consistently identified as the dominant drivers, with temperature most frequently emerging as the top contributor. As shown in Fig. S5 and S6, DNF often showed temperature or radiation as the

300 variable with the highest feature importance, whereas DBF frequently showed both temperature and precipitation among the top-ranked drivers. In MF, the secondary drivers after temperature alternated between precipitation and radiation, and no single secondary factor dominated. These patterns indicate that climatic conditions play a central role in structuring resistance and resilience in forest systems, with radiation being particularly influential in the DNF and precipitation being more important in the DBF.

305 The effects of drought on OS, S, G, C, and C/N were especially pronounced (deep red cells in Table 2). Under Severe or Extreme droughts, non-climatic variables—ASI, ASL, ASR, and elevation—often emerged as the most important drivers

rather than climate variables. These land cover types share relatively sparse or structurally constrained vegetation, which may limit their buffering capacity against water stress.

In OS and C, ASL had the highest feature importance under extreme drought at the SPEI-3 timescale, and resistance values were below 0.99, suggesting that species loss contributes to reduced drought resistance. In C, ASI was the dominant driver under extreme drought (Fig. S5–S6), indicating the potential role of introducing drought-tolerant crop varieties in shaping stability. In C/N, ASR showed the highest contribution to resistance under SPEI-6. Fig. S5–S6 indicate that this reflects the relatively strong effects of temperature and precipitation combined with the weaker influence of radiation, rather than an unusually high ASR.

Under Extreme or Severe wet conditions, both resistance and resilience exceeded 1 in these sparsely vegetated or managed land cover types, indicating enhanced vegetation functioning. In such cases, temperature-related variables are the most frequently identified leading drivers. Radiation was the most influential variable for OS resilience under SPEI-3 and SPEI-6, and elevation showed the highest feature importance for G resistance under SPEI-6.
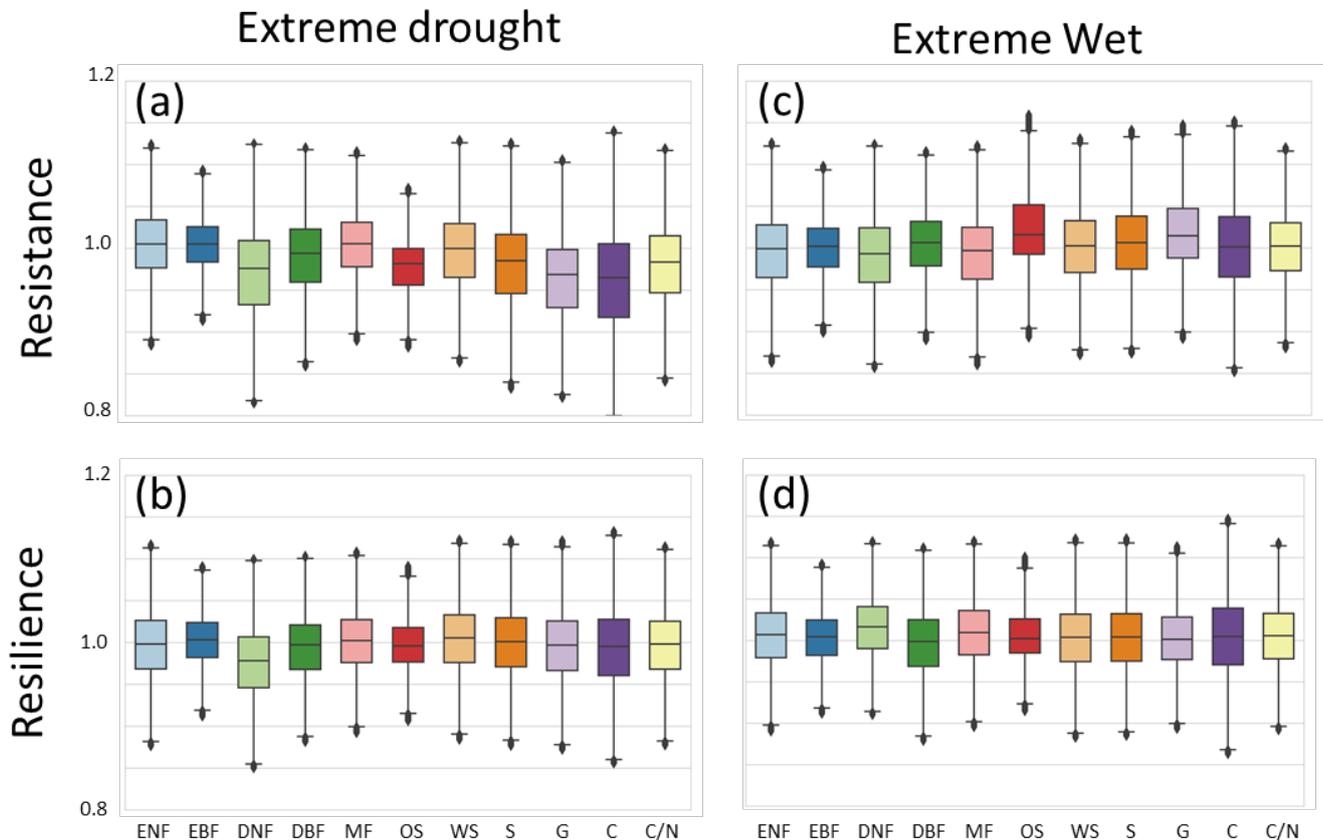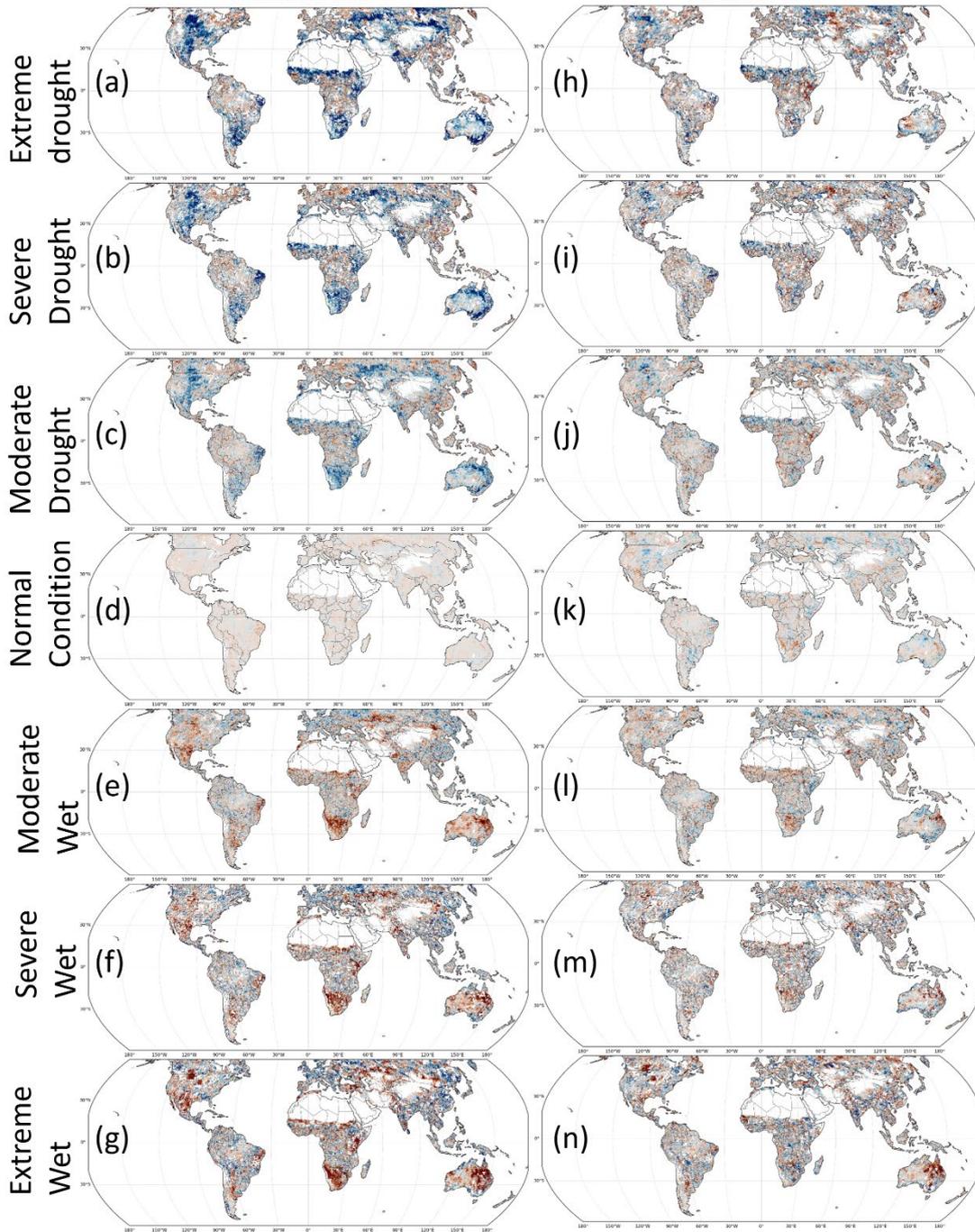

Figure 5. Boxplots of vegetation resistance for each land cover type under different SPEI-3 climate categories. For each land cover class, resistance values were aggregated across grid cells and filtered by removing statistical outliers based on the

13

interquartile range (IQR; values outside $Q1 - 1.5 \times IQR$ and $Q3 + 1.5 \times IQR$ were removed). For visualization, the values were restricted to the physiologically plausible range of 0.8–1.2. Colors were selected from 11 tones of the paired color palette to enhance the contrast among land cover types. The box edges represent the 25th and 75th percentiles, the center line indicates the median, and the whiskers extend to the most extreme non-outlier values.

SPEI-3

Resistance   Resilience

Extreme drought   (a)   (h)

Severe Drought   (b)   (i)

Moderate Drought (c)   (j)

Normal Condition (d)   (k)

Moderate Wet   (e)   (l)

Severe Wet   (f)   (m)

Extreme Wet   (g)   (n)

0.90 0.92 0.94 0.96 0.98 1.0 1.02 1.04 1.06 1.08 1.1

Table 2. Variables with the highest feature importance in the LightGBM analysis for each climate–land cover combination (resistance and resilience as response variables).

Land Cover	SPEI	Resistance							Resilience						
		EXD	SED	MOD	NOR	MOW	SEW	EXW	EXD	SED	MOD	NOR	MOW	SEW	EXW
Evergreen Needle leaf Forest	3	**T**	T-1	T	T	T	**T**	**T-1**	EI	**T-1**	T-1	T+1	T	T+1	T+1
	6	**T-1**	T-1	T-1	T-1	T-1	T	T-1	T-1	**T-1**	T-1	T-1	T+1	**T+1**	T
	12	**T**	T	T	T	T	T-1	T	T-1	**T-1**	T-1	T-1	T+1	T	T
Evergreen Broadleaf Forest	3	T	T-1	T-1	T-1	T-1	T	T-1	T+1	T-1	T-1	T-1	T	T-1	T
	6	T	T-1	T-1	T	T-1	P-1	T	T+1	T+1	T-1	T-1	T-1	T-1	T-1
	12	T	T	P-1	T-1	T-1	T	T-1	T-1	T-1	T-1	T	T-1	T+1	T-1
Deciduous Needleleaf Forest	3	**R-1**	**T-1**	**T**	**T-1**	R	**R-1**	T	**T**	**T-1**	T-1	T-1	**R+1**	**R+1**	T+1
	6	**T-1**	**T**	**T-1**	T	R	**R-1**	T	**R+1**	T	**T+1**	**T+1**	**R+1**	T-1	T+1
	12	**T-1**	**T-1**	**T-1**	**T-1**	T	**R-1**	**R-1**	**P+1**	T	T	**R+1**	**R+1**	T-1	T-1
Deciduous Broadleaf Forest	3	**T-1**	**T-1**	**T-1**	T-1	P	**T-1**	**T-1**	**T+1**	**T-1**	**T-1**	T	**T+1**	T	T
	6	**T-1**	**T-1**	**T**	T-1	**T-1**	**T-1**	T	**T-1**	**T+1**	**T+1**	**T+1**	**T+1**	**T+1**	P
	12	**T-1**	**T-1**	**P**	T-1	**T-1**	**T-1**	**T-1**	**R**	**P-1**	**T-1**	**T+1**	**T+1**	P	P
Mixed Forest	3	**T**	T	T	T	T-1	**T-1**	**T-1**	**R+1**	**T-1**	**R+1**	**T+1**	T-1	**T+1**	P
	6	**T**	T	T	T	T	**T-1**	**T**	**T**	T	T-1	**T+1**	T-1	**T+1**	**T+1**
	12	**T**	**T**	T-1	T	T	**T**	**T**	T	T	T-1	T-1	**T+1**	**T+1**	**T+1**
Open Shrubland	3	**ASL**	**T-1**	T	T	**T-1**	**T-1**	**T-1**	**T-1**	**R-1**	**T+1**	T	**T+1**	T	**R-1**
	6	**T**	**P-1**	**T-1**	T	**T-1**	**T-1**	**T-1**	**T+1**	**T**	T	**T+1**	**T+1**	**T+1**	**R+1**
	12	**T-1**	**T**	**T-1**	T	**T-1**	**T**	**T-1**	**T-1**	**T**	T	**T+1**	**T**	**T+1**	**T-1**
Woody Savanna	3	**T**	T-1	T-1	T-1	T-1	T-1	ASR	T-1	T-1	T-1	T-1	T-1	T	**T**
	6	**T**	T-1	T-1	T-1	T	T-1	**ASR**	T-1	T-1	T+1	T+1	T+1	T-1	**T+1**
	12	T	T	T-1	T-1	T-1	T-1	R	T-1	T	T	T+1	T-1	T+1	T+1

Land type		V1	V2	V3	V4	V5	V6	V7		V1	V2	V3	V4	V5	V6	V7
Savanna	3	**T**	**T-1**	T-1	T-1	**T-1**	**T-1**	**T-1**		**T**	**T**	T+1	T+1	R+1	**T-1**	**T+1**
	6	**T-1**	**ASI**	T-1	T-1	T-1	**T-1**	**T-1**		**T-1**	**T-1**	T+1	T+1	T+1	**T-1**	**T**
	12	**T-1**	**T-1**	T-1	T-1	T-1	**T-1**	**T-1**		**T-1**	**T+1**	T+1	T+1	T+1	**T+1**	**T+1**
Grassland	3	**ASL**	**El**	T	T	**T**	**T**	**El**		**T+1**	**T-1**	T+1	T+1	T-1	P	**T+1**
	6	**El**	**El**	T	T	**T**	**T**	**T**		**T-1**	**T**	T	T	T-1	T-1	**T**
	12	**ASL**	T-1	T	T	**T**	**T**	T-1		**T-1**	**T**	T	T	T-1	T	**T**
Cropland	3	**ASI**	**T**	T-1	T-1	T	**T**	**T-1**		**T-1**	**T-1**	P-1	T-1	T+1	**P-1**	**T-1**
	6	**ASI**	**T-1**	T-1	T-1	T-1	**T**	**T**		**T+1**	**T-1**	T+1	T+1	T+1	**T-1**	**T**
	12	**ASI**	**T**	T-1	T	T-1	**T-1**	**T-1**		**T+1**	**T-1**	T-1	T	T+1	**T-1**	**T+1**
Cropland/Natural vegetation mosaic	3	**P**	T	T	T-1	T-1	T-1	T		T-1	T-1	T-1	T+1	T+1	T-1	T+1
	6	**ASR**	T	T-1	T	T-1	T	T-1		T-1	T-1	T-1	T	T+1	T-1	T
	12	**T**	T	T-1	T-1	T-1	T	T		T-1	T-1	T-1	T-1	T+1	T+1	T+1

Note. Each string represents an explanatory variable (Fig. 1). Bold text indicates models with a coefficient of determination (R^2) of ≥ 0.5. The background pattern of each cell indicates the magnitude of resistance or resilience. Values between 0.99 and 1 (inclusive of 0.99 and exclusive of 1) are shown with light diagonal hatching slanting downward to the right. Values greater than 1 and up to 1.01 (inclusive of 1 and 1.01) are indicated with a gray background. Values below 0.99 are represented by dark diagonal hatching slanting downward to the right, whereas values above 1.01 are shown with dark diagonal hatching slanting upward to the right. T, P, and R denote temperature, precipitation, and relative humidity, respectively. The suffix −1 refers to the year preceding the climate event, and +1 refers to the year following the event. El is the elevation, ASR is the anthropogenic species richness, ASI is the anthropogenic species increase, and ASL is the anthropogenic species loss.
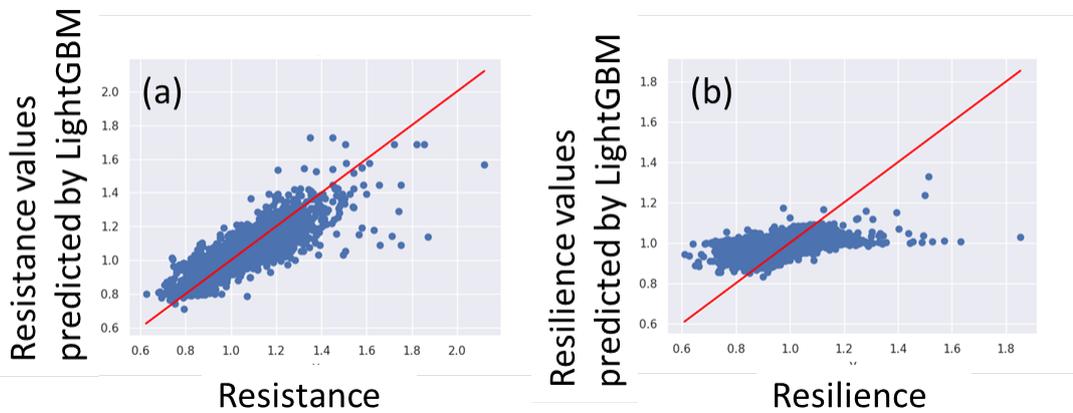
Figures 7. Examples of the model performance. (a) Highest R^2 (0.71) for resistance and (b) lowest R^2 (0.18) for resilience obtained when comparing the observed resistance (x-axis) with the resistance estimated by LightGBM (y-axis). The red line represents the 1:1 line, indicating perfect agreement between observed and predicted values.

4 Discussion

4.1 Variability Characteristics of Resistance and Resilience

Our results revealed that vegetation resistance declines markedly during droughts, particularly in arid and semi-arid regions (OS, S, G), whereas resilience exhibits weaker and less spatially coherent declines. Deciduous needle-leaf forests (DNF) consistently show low resistance and resilience, indicating high sensitivity to hydroclimatic variability. This finding is consistent with previous studies reporting reduced ecosystem stability or increased ecosystem degradation in DNF under drought and precipitation variability (Hai et al., 2025; Li et al., 2021; Nogovitcyn et al., 2023). Regions where both stability components are low are likely to experience heightened ecological vulnerability, as reduced resistance and resilience imply a diminished capacity to withstand and recover from climatic disturbances (Yao et al., 2024). Accordingly, our findings suggest that DNF may become increasingly vulnerable under future climate change scenarios.

Sparse vegetation systems, such as open shrublands (OS), grasslands (G), and croplands (C), also exhibit low resistance but maintain comparatively high resilience (Fig. 5b and d). Mapping stability across climatic categories demonstrates substantial spatial heterogeneity in ecosystem responses, highlighting that ecosystem do not respond uniformly to droughts or heavy rainfall. Even under similar climatic conditions and within the same land-cover type, resistance and resilience responses to extreme climatic events can vary markedly. This spatial heterogeneity is consistent with previous findings that sparse vegetation, although highly vulnerable to immediate drought impacts, often exhibits rapid post-drought recovery (Ponce-Campos et al., 2013; Seddon et al., 2016). The pronounced spatial heterogeneity observed in this study underscores the necessity of evaluating ecosystem stability within comparable climatic contexts rather than generalizing responses across biomes or land cover types.

4.2 Feature Importance of Resistance and Resilience Across Climatic Gradients

Temperature emerged as the dominant driver of both resistance and resilience under normal climatic conditions. Although this result partially overlaps with the findings of Huang and Xia (2019), a direct comparison is difficult because the climatic gradient classifications differ. The strong influence of temperature is consistent with studies reporting temperature-driven vegetation shifts and abrupt transitions in ecosystem functioning (Berdugo et al. 2022). Resistance was most strongly associated with temperature in the previous year (T−1), supporting the concept that ecosystems undergo "pre-conditioning" based on antecedent thermal and soil moisture conditions (De Keersmaecker et al., 2015; Fu et al., 2024). In contrast, resilience, the capacity to recover following disturbance, is best explained by temperature in the year after the event (T+1), reflecting the temperature sensitivity of root and shoot regrowth processes (Wu et al., 2025). These patterns reinforce that resistance and resilience reflect ecologically distinct mechanisms governed by antecedent and recovery-year conditions.

In ENF, EBF, and WS, neither resistance nor resilience exhibited clear climatic signals. This absence likely reflects strong ecological buffering mechanisms, such as conservative leaf traits, deep-rooting systems, or high internal water storage, which dampen interannual variability in response to extreme events (Seddon et al., 2016). Because the amplitude of interannual variation in these systems is small, statistical models such as LightGBM may be unable to capture substantial explained variance, resulting in R^2 values below 0.5 for some combinations. In this sense, muted climatic responses should not be interpreted as ecological insensitivity but as evidence that biological and structural traits reduce the detectability of climate-driven variations in remote-sensing datasets.

Under Severe and Extreme drought conditions, non-climatic variables, particularly anthropogenic species increase (ASI), species loss (ASL), species richness (ASR), and elevation, frequently emerged as the dominant drivers. This shift highlights the increasing role of biotic and structural attributes when water availability becomes extremely limited. Even small changes in species composition or vegetation structure can substantially alter resistance or resilience to severe stress. For example, high ASL values in grasslands and open shrublands coincided with resistance values below 0.99 under extreme drought, suggesting that biodiversity loss directly reduces drought resistance. This finding is consistent with earlier research demonstrating that higher biodiversity enhances stability under extreme climatic events (Isbell et al., 2015) and emphasizes that human-induced biodiversity loss increases vulnerability in sparse vegetation systems.

In croplands, ASI was the most important variable during extreme droughts. This result reflects the influence of management-dependent species turnover; the introduction or expansion of drought-tolerant cultivars can substantially alter ecosystem resistance. This observation aligns with agronomic studies showing that cultivar selection plays a critical role in modulating crop productivity and stability under drought conditions (Lobell et al., 2014). These results collectively highlight the complex interplay between climatic and biotic factors and emphasize the relevance of accounting for species composition, trait diversity, and land management practices when assessing the ecosystem stability.

Overall, the results indicate that the mechanisms governing ecosystem stability shift substantially along the climatic severity gradient. Under Normal conditions, temperature primarily regulates both resistance and resilience. Under Severe and Extreme droughts, climatic controls weaken, and biotic and structural characteristics become the primary determinants of ecosystem responses. These findings demonstrate that climatic variables alone are insufficient for predicting vegetation stability under intense water limitation and that ecological and structural traits must be incorporated into the predictive frameworks.

4.3 Limitations

Despite the strengths of this study, several limitations should be acknowledged. First, the temporal discontinuity caused by excluding NDVI observations from 1990 to 1994 may reduce the continuity of long-term trends, even though this step was necessary to avoid artifacts stemming from NOAA-11 orbital drift and the Pinatubo eruption. Second, the biodiversity indicators (ASI, ASL, and ASR) and long-term land-use reconstructions (HYDE 3.1) rely on modeled estimates and contain inherent uncertainties that may influence the relative importance of explanatory variables. Third, LightGBM identifies statistical associations rather than causal mechanisms, and spatial autocorrelation among grid cells may affect the model

performance even with large datasets. Fourth, relying solely on NDVI as a proxy for vegetation functioning may underestimate productivity changes in high-biomass systems because of canopy saturation. Fifth, climatic variables were aggregated to calendar-year values, which may introduce uncertainty in regions with pronounced wet–dry seasonality, where the definition of an annual period can artificially split wet or dry seasons across years and potentially dampen or distort climate signals relevant to ecosystem responses, particularly in monsoonal and seasonally dry ecosystems. Future research incorporating longer observational records, improved biodiversity and soil datasets, alternative vegetation indices, and more detailed land-use histories will help address these limitations and enable more robust assessments of ecosystem stability during extreme climatic events.

5 Conclusion

This study demonstrates that the controls on ecosystem stability vary systematically with the severity of hydroclimatic extremes. By integrating NDVI-based resistance and resilience metrics with climate classifications derived from SPEI and a machine-learning framework, we showed that temperature and precipitation dominate ecosystem stability under Normal and Moderate climatic conditions. Resistance is largely shaped by antecedent temperature, whereas resilience is governed by temperature during the recovery year, reflecting the mechanistic distinction between susceptibility and recuperation.

However, as drought severity increases, the influence of climatic factors diminishes in many regions. Under Severe and Extreme droughts, biotic and structural variables, including anthropogenic species loss, species increase, species richness, and elevation, become the primary determinants of stability. These effects are most pronounced in sparsely vegetated systems, such as open shrublands, grasslands, and croplands. In contrast, deciduous needle-leaf forests exhibit consistently low resistance and resilience across climatic conditions, highlighting their heightened vulnerability to future climate variability.

The spatial patterns of resistance and resilience reveal substantial heterogeneity within and across biomes, underscoring the need to evaluate stability under comparable climatic regimes rather than relying on biome-level generalizations alone. A major contribution of this study is its climate-explicit integrative framework, which jointly considers climatic, biotic, edaphic, topographic, and long-term land-use factors. This approach provides the first global-scale evidence that the dominant controls of vegetation stability shift from meteorological to biotic and structural drivers as drought intensifies.

Our results indicate that approaches relying solely on climatic variables are insufficient for predicting ecosystem behavior under extreme conditions. Therefore, management strategies aimed at enhancing ecological stability must incorporate the interacting influences of biodiversity, vegetation structure, land-use history, and local site conditions. Although the available datasets impose temporal and thematic limitations, this study highlights key directions for improving global assessments of ecosystem stability, including longer observational records, enhanced biodiversity and soil datasets, and refined reconstructions of historical land use patterns.

Please use only the styles of this template (MS title, Authors, Affiliations, Correspondence, Normal for your text, and Headings 1–3). The title page must include the title (concise but informative), author first and last names, full institutional addresses of

all authors, and correspondence email for proofs. Deceased co-authors should be marked accordingly. After the abstract, the sequence of the sections of your manuscript is introduction, sections of your choice, and conclusions.

Code, data, or code and data availability

All data used in this analysis are cited throughout the manuscript: land cover type (Channan et al., 2014), potential evapotranspiration (University of East Anglia Climatic Research Unit et al., 2017), precipitation (Schneider, 2015), NDVI (Mao and Yan, 2019), temperature (University of East Anglia Climatic Research Unit et al., 2017), radiation (European Centre for Medium-Range Weather Forecasts, 2012), Species richness (Ellis et al., 2012), Land use history (Klein Goldewijk et al., 2011), Irrigation(Siebert et al., 2013) , Elevation (Fischer et al., 2008) and Soil properties (Global Soil Data Task Group. (2000). The code to conduct this analysis is published in a separate Zenodo repository (Yanagawa et al., 2026).

Supplement link

The supplementary material is currently included at the end of the manuscript; however, it will be provided separately in its final version.

Author contributions

No competing interests

Financial support

References

Adler, P. B., Milchunas, D. G., Lauenroth, W. K., Sala, O. E., and Burke, I. C.: Functional traits of graminoids in semi-arid steppes: A test of grazing histories, J. Appl. Ecol., 41, 653–663, https://doi.org/10.1111/j.0021-8901.2004.00934.x, 2004.

Beck, P. S. A., Atzberger, C., Høgda, K. A., Johansen, B., and Skidmore, A. K.: Improved monitoring of vegetation dynamics at very high latitudes: A new method using MODIS NDVI, Remote Sens. Environ., 100, 321–334, https://doi.org/10.1016/j.rse.2005.10.021, 2006.

Beguería, S. and Vicente-Serrano, S. M.: SPEI: Calculation of the Standardized Precipitation–Evapotranspiration Index [software], http://sac.csic.es/spei, 2017.

Berdugo, M., Gaitán, J. J., Delgado-Baquerizo, M., Crowther, T. W., and Dakos, V.: Prevalence and drivers of abrupt vegetation shifts in global drylands, Proc. Natl. Acad. Sci. USA, 119, e2123393119, https://doi.org/10.1073/pnas.2123393119, 2022.

Channan, S., Collins, K., and Emanuel, W. R.: Global mosaics of the standard MODIS land cover type data, University of Maryland and Pacific Northwest National Laboratory [data set], http://www.qgistutorials.com/downloads/LC_hd_global_2012.tif.gz, 2014.

Chen, J., Chi, Y., Zhou, W., Wang, Y., Zhuang, J., Zhao, N., et al.: Quantifying the dimensionalities and drivers of ecosystem stability at global scale, J. Geophys. Res.-Biogeosci., 126, e2020JG006041, https://doi.org/10.1029/2020JG006041, 2021.

De Keersmaecker, W., Lhermitte, S., Tits, L., Honnay, O., Somers, B., and Coppin, P.: A model quantifying global vegetation resistance and resilience to short-term climate anomalies and their relationship with vegetation cover, Global Ecol. Biogeogr., 24, 539–548, https://doi.org/10.1111/geb.12279, 2015.

Ellis, E. C., Antill, E. C., and Kreft, H.: All is not loss: plant biodiversity in the Anthropocene, PLoS ONE, 7, e30535, https://doi.org/10.1371/journal.pone.0030535, 2012.

European Centre for Medium-Range Weather Forecasts: ERA-Interim Project, Monthly Means, NSF National Center for Atmospheric Research [data set], https://doi.org/10.5065/D68050NT, 2012.

Forzieri, G., Dakos, V., McDowell, N. G., et al.: Emerging signals of declining forest resilience under climate change, Nature, 608, 534–539, https://doi.org/10.1038/s41586-022-04959-9, 2022.

510

Fu, C., Hao, H., Li, T., Li, Y., and Yang, F.: Lag effects of vegetation temperature stress and its ecological risk assessment, Front. Environ. Sci., 12, 1424578, https://doi.org/10.3389/fenvs.2024.1424578, 2024.

Global Soil Data Task Group: Global gridded surfaces of selected soil characteristics (IGBP-DIS), ORNL DAAC [data set], 515 https://doi.org/10.3334/ORNLDAAC/569, 2000.

Hai, Y., Han, T., Wang, Y., Li, R., Yang, Y., Wen, Z., and Zheng, H.: Quantifying the impact of precipitation fluctuations on forest growth in Northeast China, Front. Plant Sci., 16, 1570005, https://doi.org/10.3389/fpls.2025.1570005, 2025.

520 Holling, C. S.: Resilience and stability of ecological systems, Annu. Rev. Ecol. Syst., 4, 1–23, https://doi.org/10.1146/annurev.es.04.110173.000245, 1973.

Huang, K. and Xia, J.: High ecosystem stability of evergreen broadleaf forests under severe droughts, Global Change Biol., 25, 3494–3503, https://doi.org/10.1111/gcb.14748, 2019.

525

Isbell, F., Craven, D., Connolly, J., Loreau, M., Schmid, B., Beierkuhnlein, C., et al.: Biodiversity increases the resistance of ecosystem productivity to climate extremes, Nature, 526, 574–577, https://doi.org/10.1038/nature15374, 2015.

Justice, C. O., Townshend, J. R. G., Holben, B. N., and Tucker, C. J.: Analysis of the phenology of global vegetation using 530 meteorological satellite data, Int. J. Remote Sens., 6, 1271–1318, https://doi.org/10.1080/01431168508948281, 1985.
Kreft, H. and Jetz, W.: Global patterns and determinants of vascular plant diversity, Proc. Natl. Acad. Sci. USA, 104, 5925–5930, https://doi.org/10.1073/pnas.0608361104, 2007.

Klein Goldewijk, K., Beusen, A., van Drecht, G., and de Vos, M.: The HYDE 3.1 spatially explicit database of human-induced 535 global land-use change over the past 12,000 years, Global Ecol. Biogeogr., 20, 73–86, https://doi.org/10.1111/j.1466-8238.2010.00587.x, 2011.

Li, D., Wu, S., Liu, L., Zhang, Y., and Li, S.: Vulnerability of the global terrestrial ecosystems to climate change, Global Change Biol., 24, 4095–4106, https://doi.org/10.1111/gcb.14327, 2018.

540

Li, X., Yao, Y., Yin, G., Peng, F., and Liu, M.: Forest resistance and resilience to the 2002 drought in northern China, Remote Sens., 13, 2919, https://doi.org/10.3390/rs13152919, 2021.

545 Lobell, D. B., Roberts, M. J., Schlenker, W., Braun, N., Little, B. B., Rejesus, R. M., and Hammer, G. L.: Greater sensitivity to drought accompanies maize yield increase in the U.S. Midwest, Science, 344, 516–519, https://doi.org/10.1126/science.1251423, 2014.

Mao, J. and Yan, B.: Global monthly mean leaf area index climatology, 1981–2015, ORNL DAAC, Oak Ridge, Tennessee, USA [data set], https://doi.org/10.3334/ORNLDAAC/1653, 2019.

550 Mori, A. S., Furukawa, T., and Sasaki, T.: Response diversity determines the resilience of ecosystems to environmental change, Biol. Rev., 88, 349–364, https://doi.org/10.1111/brv.12004, 2013.

Nogovitcyn, A., Shakhmatov, R., Morozumi, T., Tei, S., Miyamoto, Y., Shin, N., et al.: Historical variation in the normalized 555 difference vegetation index compared with soil moisture in a taiga forest ecosystem in northeastern Siberia, Biogeosciences, 20, 3185–3201, https://doi.org/10.5194/bg-20-3185-2023, 2023.

Ponce-Campos, G. E., Moran, M. S., Huete, A., Zhang, Y., Bresloff, C., Huxman, T. E., et al.: Ecosystem resilience despite large-scale altered hydroclimatic conditions, Nature, 494, 349–352, https://doi.org/10.1038/nature11836, 2013.

560 Ripple, W. J., Wolf, C., Gregg, J. W., Rockström, J., Mann, M. E., Oreskes, N., et al.: The 2024 state of the climate report: Perilous times on planet Earth, BioScience, 74, 812–824, https://doi.org/10.1093/biosci/biae087, 2024.

Schneider, U., Becker, A., Finger, P., Meyer-Christoffer, A., Rudolf, B., and Ziese, M.: GPCC full data monthly product 565 version 7.0 at 0.5°: Monthly land-surface precipitation from rain gauges built on GTS-based and historic data, Global Precipitation Climatology Centre (GPCC), Deutscher Wetterdienst (DWD) [data set], https://doi.org/10.5676/DWD_GPCC/FD_M_V7_050, 2015.

Seddon, A. W. R., Macias-Fauria, M., Long, P. R., Benz, D., and Willis, K. J.: Sensitivity of global terrestrial ecosystems to 570 climate variability, Nature, 531, 229–232, https://doi.org/10.1038/nature16986, 2016.

Shi, Y., Kong, G., Soukhavong, D., Lamb, J., Meng, Q., Finley, T., et al.: lightgbm: Light Gradient Boosting Machine (version 4.6.0.99) [R package], https://github.com/Microsoft/LightGBM, 2025.

575   Siebert, S., Henrich, V., Frenken, K., and Burke, J.: Global map of irrigation areas version 5, Rheinische Friedrich-Wilhelms-Universität Bonn and Food and Agriculture Organization of the United Nations, Rome [data set], https://firebasestorage.googleapis.com/v0/b/fao-aquastat.appspot.com/o/GIS%2Fgmia_v5_aei_pct_asc.zip, 2013.

Smith, T., Traxl, D., and Boers, N.: Empirical evidence for recent global shifts in vegetation resilience, Nature Climate Change, 12, 477–484, https://doi.org/10.1038/s41558-022-01352-2, 2022.
580

Smith, T. and Boers, N.: Global vegetation resilience linked to water availability and variability, Nature Communications, 14, 498, https://doi.org/10.1038/s41467-023-36207-7, 2023.

585   Sun, N., Liu, N., Zhao, X., Zhao, J., Wang, H., and Wu, D.: Evaluation of spatiotemporal resilience and resistance of global vegetation responses to climate change, Remote Sens., 14, 4332, https://doi.org/10.3390/rs14174332, 2022.

University of East Anglia Climatic Research Unit, Harris, I. C., and Jones, P. D.: CRU TS4.01: Climatic Research Unit (CRU) time-series (TS) version 4.01 of high-resolution gridded data of month-by-month variation in climate (Jan 1901–Dec 2016),
590   Centre for Environmental Data Analysis [data set], https://doi.org/10.5285/58a8802721c94c66ae45c3baa4d814d0, 2017.

van Meerbeek, K., Jucker, T., and Svenning, J.-C.: Unifying the concepts of stability and resilience in ecology, J. Ecol., 109, 3114–3132, https://doi.org/10.1111/1365-2745.13651, 2021.

595   Vicente-Serrano, S. M., Beguería, S., and López-Moreno, J. I.: A multiscalar drought index sensitive to global warming: the Standardized Precipitation Evapotranspiration Index, J. Climate, 23, 1696–1718, https://doi.org/10.1175/2009JCLI2909.1, 2010.

Vogel, A., Scherer-Lorenzen, M., and Weigelt, A.: Grassland resistance and resilience after drought depends on management
600   intensity and species richness, PLoS ONE, 7, e36992, https://doi.org/10.1371/journal.pone.0036992, 2012.

Wei, M., Li, S., Zhu, L., Lu, X., Li, H., and Feng, J.: Continuous abrupt vegetation shifts in the global terrestrial ecosystem, Ecol. Lett., 28, e70069, https://doi.org/10.1111/ele.70069, 2025.

605   Wu, G., Jiang, L., Li, Q., Tan, Z., Liu, W., and Gui, X.: Higher post-drought recovery capacity of vegetation productivity compared to greenness in Central Asia, J. Environ. Manage., 390, 126214, https://doi.org/10.1016/j.jenvman.2024.126214, 2025.

Yanagawa, A., Yoshikawa, S., Iseri, Y., Ueda, R., and Kanae, S.: Drivers of resistance and resilience under different intensities

610   of extreme climatic events (version 1.0), Zenodo [data set], https://doi.org/10.5281/zenodo.18428493, 2026.

The data are not yet publicly released; however, they are available to reviewers during the review period through the following link.

(https://zenodo.org/records/18428493?preview=1&token=eyJhbGciOiJIUzUxMiIsImlhdCI6MTc2OTg5NzI3OSwiZXhwIjo

xODMwMjExMTk5fQ.eyJpZCI6IjFhYTM2OGVhLTg5ZmQtNGYxMS1hMjIyLWYxZmJjN2U3YTczOCIsImRhdGEiOnt

615   9LCJyYW5kb20iOiI1OTk4OWJjMDc0ODM5NjRhYjNlZDQyM2NmZWY1ZjljOSJ9.yUQ0nkhMCCMlHfiAfJgzn5bu1wd

LRn0O8eUa4eMcTMJY2C_cifO_kRHfq3ZI-_rpKQkHN6PmdX9iJCYzEO8QHQ)

Yao, Y., Liu, Y., Song, J., Tao, S., Li, Y., Wu, T., et al.: Declining tradeoff between resistance and resilience of ecosystems to drought, Earth's Future, 12, e2024EF004665, https://doi.org/10.1029/2024EF004665, 2024.

620